IEEE Access
Multidisciplinary ⋮ Rapid Review ⋮ Open Access Journal

Received 18 February 2025, accepted 6 April 2025, date of publication 15 April 2025, date of current version 20 May 2025.

Digital Object Identifier 10.1109/ACCESS.2025.3561166

RESEARCH ARTICLE

Enhanced Carbon Flux Forecasting via STL Decomposition and Hybrid ARIMA-ES-LSTM Model in Amazon Forest

JEAN A. C. DIAS[1], PEDRO H. DO V. GUIMARÃES[1], WILLIANE G. S. PEREIRA[1], LEONARDO DE O. TAMASAUSKAS[1], MARIVAN S. GOMES[2], ALAN B. S. CORRÊA[1,3], KARLA FIGUEIREDO[4], GILSON COSTA[5], (Member, IEEE), GABRIEL BRITO COSTA[6,7,8,9,10], FERNANDO A. R. COSTA[1,11], AND MARCOS C. DA R. SERUFFO[1,3,12]

[1]Operational Research Laboratory, Federal University of Pará (UFPA), Belém 66075-110, Brazil
[2]School of Technology, State University of Amazonas (UEA), Amazonas 69850-000, Brazil
[3]Post-Graduate Program in Electrical Engineering (PPGEE), Federal University of Pará (UFPA), Belém 66075-110, Brazil
[4]Department of Informatics and Computer Science, Institute of Mathematics and Statistics, Rio de Janeiro State University (UERJ), Rio de Janeiro 20550-013, Brazil
[5]Department of Genetics, Institute of Biological and Health Sciences II, Rio de Janeiro State University (UERJ), Rio de Janeiro 20550-013, Brazil
[6]Post-Graduate Program in Natural Resources of the Amazon (PPGRNA), Federal University of Western Pará (UFOPA), Santarém 68035-110, Brazil
[7]Climate Sciences Post-Graduate Program, Federal University of Rio Grande do Norte, Natal, Rio Grande do Norte 59078-970, Brazil
[8]Biosciences Post-Graduate Program (PPGBIO), Federal University of Western Pará (UFOPA), Santarém, Pará 68035-110, Brazil
[9]Post-Graduate Program in Forest Science, Technology and Innovation-PPGCTIF, Federal University of Western Pará (UFOPA), Santarém, Pará 68035-110, Brazil
[10]Biotechnology and Biodiversity–Bionorte Network (REDE BIONORTE), Federal University of Western Pará (UFOPA), Santarém, Pará 68035-110, Brazil
[11]Post-Graduate Program in Sustainable Development of the Humid Tropics (PPGDSTU), Center for High Amazonian Studies (NAEA), Federal University of Pará (UFPA), Belém, Pará 66075-110, Brazil
[12]Post-Graduate Program in Anthropic Studies in the Amazon (PPGEAA), Federal University of Pará (UFPA), Castanhal, Pará 68746-630, Brazil

Corresponding author: Alan B. S. Corrêa (alan.correa@itec.ufpa.br)

This work was supported in part by the Programa de Bolsas de Produtividade em Pesquisa e Desenvolvimento Tecnológico-Universidade Federal do Oeste do Pará (PQDT-UFOPA) to G. B.-C., through Research Incentive Program-Programa de Incentivo à Pesquisa (PIP) [Programa de Pós-Graduação em Biociências (PPBIO)-UFOPA]; in part by the Granting of Financial Aid for Research (PPGRNA-UFOPA); in part by Coordenação de Aperfeiçoamento de Pessoal de Nível Superior (CAPES)-Código de Financiamento under Grant 001; in part by Conselho Nacional de Desenvolvimento Científico e Tecnológico (CNPQ); in part by Financiadora de Estudos e Projetos (FINEP) and Universidade Federal do Pará (UFPA); in part by AmeriFlux data were made available through the data portal (https://ameriflux.lbl.gov) and processing maintained by the AmeriFlux Management Project, funded by U.S. Department of Energy Office of Science, Office of Biological and Environmental Research, under Contract DE-AC02-05CH11231; and in part by the Coordination for the Improvement of Higher Education Personnel-CAPES under Grant ROR identifier: 00x0ma614.

ABSTRACT This study presents a hybrid model, STL-ARIMA-ES-LSTM, developed to improve the accuracy of Gross Primary Productivity (GPP) forecasts in the Amazon region. The model integrates seasonal and trend decomposition using Loess (STL) with statistical methods (ARIMA and Exponential Smoothing-ES) and a machine learning technique (Long Short-Term Memory - LSTM). Applied to GPP data from the PE-QFR site, the hybrid model achieved significantly better error metrics, with RMSE of 1.69 gC/m^2/day, MAE of 1.35 gC/m^2/day, and MAPE of 0.20%, compared to the standalone LSTM (RMSE of 2.16 gC/m^2/day, MAE of 1.78 gC/m^2/day, and MAPE of 0.27%). Furthermore, the hybrid model showed stronger agreement with the observed data, with correlation coefficient r = 0.62 and R^2 = 0.39, whereas the LSTM alone yielded r = 0.26 and R^2 = –0.002. The STL decomposition allowed effective separation of trend, seasonality, and residual components, enabling tailored modeling of each, which contributed to the improved predictive performance. These results demonstrate the advantage of hybrid approaches in capturing the nonlinear and seasonal patterns of GPP, supporting enhanced environmental monitoring and more informed climate change mitigation strategies in the Amazon.

The associate editor coordinating the review of this manuscript and approving it for publication was Chaitanya U. Kshirsagar.

INDEX TERMS Gross primary productivity, carbon flux, hybrid models, STL decomposition, LSTM, statistical models, amazon forest.

I. INTRODUCTION

Climate change, driven primarily by carbon dioxide (CO_2) emissions, stands as one of the greatest environmental and socioeconomic threats of the 21st century [1]. The increasing accumulation of this gas in the atmosphere significantly contributes to global temperature rise, intensifying the occurrence of extreme weather events such as heatwaves, heavy rainfall, floods, and prolonged droughts [2], [3], [4]. These phenomena have profound impacts on both the environment and human activities, including water resource scarcity, increased respiratory diseases, threats to food security, among others [4], [5], [6], [7], [8].

In this context, the Amazon plays a crucial role in global and regional climate regulation, acting as an important CO_2 sink, contributing to reducing its concentration in the atmosphere [9], [10], [11]. However, the growing pressure caused by forest degradation, deforestation and the lack of effective public policies jeopardize the forest's ability to mitigate the effects of climate change [12], [13], [14]. Given this scenario, understanding and forecasting carbon fluxes becomes essential to anticipate trends and support more effective conservation strategies.

The forecasting of these fluxes is closely linked to the estimation of Gross Primary Productivity (GPP), which represents the carbon fixed by plants during photosynthesis and serves as a key indicator of ecosystem functioning [15]. By reflecting the forest's response to physical and biological disturbances, GPP is a critical variable for understanding energy flow within an ecosystem [8], [16], [17]. However, accurate prediction of GPP is challenged by its high interannual variability and sensitivity to extreme climatic conditions [9], [18], [19], [20], which may distort the understanding of its future behavior in the region.

To estimate GPP, techniques such as eddy covariance (EC) are widely used, enabling in situ monitoring of carbon fluxes through stations known as flux towers [9], [21], [22]. However, the low density of towers in the Amazon, in addition to the limited range of measurements made by these structures, reduces the effectiveness of large-scale forecasts of these flux variables due to the vastness of the region [23], [24].

In this context, the use of remote sensing data has become essential for monitoring and predicting GPP in a viable and effective way in larger regions due to its wide range [16], [21], [25]. One example is the MOD17 product from the Moderate-Resolution Imaging Spectroradiometer (MODIS) satellite, which provides data at a resolution of 500 meters from the earth's surface every 8 days [26], [27], making it crucial to understand the behavior of this variable in regions inaccessible by field measurements or flux towers.

However, although remote sensing provides essential data, accurate GPP forecasting—especially considering its significant spatial and temporal variations [28], requires more sophisticated approaches. In this regard, Artificial Intelligence (AI)-based methods have been widely applied to estimate environmental variables such as GPP, demonstrating considerable potential in forecasting this variable [29], [30], [31]. This potential is particularly evident in AI's ability to deal with non-linear and complex problems, common characteristics in forest ecosystems, where interactions between the various environmental factors can be highly dynamic [18].

In this context, [32] compared three neural network architectures for daily GPP forecasting — Recurrent Neural Networks (RNNs), Gated Recurrent Units (GRUs), and Long Short-Term Memory (LSTMs) — observing similar performance among the models, but with LSTMs standing out for their lower error rates in predicting extreme GPP values induced by climate. Other studies reinforce the effectiveness of LSTMs in modeling environmental time series: [33] achieved good results in temperature forecasting, while [34] proposed the AELSTM model, based on LSTMs, which outperformed traditional approaches in estimating vegetation cover. Collectively, these studies highlight the potential of LSTMs in forecasting complex environmental variables and suggest that they may yield promising results in GPP estimation.

In addition to AI models, statistical methods have also been applied in forecasting environmental variables with satisfactory results. In [35], the ARIMA model was used to estimate GPP in China, showing good performance in most regions, although with limitations in areas with lower data quality. Meanwhile, [36] compared ARIMA, Double Exponential Smoothing (DES), and Grey Model (GM) for forecasting greenhouse gas emissions in Turkey, with DES proving to be the most effective, followed by ARIMA and, finally, GM. These results suggest that both ARIMA and DES can be considered promising methods for GPP forecasting, especially in contexts with consistent historical data.

In order to refine the forecasting of statistical methods, the study by [37] investigated the integration of the Seasonal and Trend decomposition using Loess (STL), which, by separating the time series into simpler components, facilitates modeling, especially for seasonality. However, it was observed that this approach might compromise the performance of AI models, which already capture complex patterns in an integrated way and are hindered by the separation of the data. However, the study did not investigate the possibility of combining statistical and AI models, hybrid models [38], [39], [40], to treat each part of the STL decomposition distinctly, which opens avenues for future research.

In this regard, [38] proposed a hybrid STL-AR-LSTM-ATLSTM model to forecast wind speed, which combines STL decomposition with ARIMA and attention-based LSTM (AT-LSTM) models. The model uses LSTM to decompose

the series into components such as trend, seasonality, and residuals, while the ARIMA-LSTM models the trend, and the AT-LSTM captures the seasonal and residual terms. The results showed superior performance compared to ARIMA, AT-LSTM, and ARIMA-AT-LSTM when used in isolation, especially in extreme values. Although the study focused on wind speed forecasting, its results highlight the potential of hybrid models in the analysis of climatic time series, paving the way and encouraging the application of similar methodologies to other variables.

Building on these foundations, this paper proposes and evaluates a hybrid model, STL-ARIMA-ES-LSTM, for forecasting GPP at the PE-QRF monitoring site located in the Peruvian Amazon, using the decomposition of time series data from the MERRA-2 and MOD15A2H satellites. The model integrates the STL decomposition technique with statistical models (ARIMA and ES) and neural networks (LSTM), enabling the isolated analysis of GPP time series components [41], [42], [43].

The contributions of this work are: i) improvement in understanding dynamics of the carbon cycle in a biome of the Amazon Ecoregion; ii) the use of state-of-the-art techniques to create more accurate and reliable modeling and forecasting methods for GPP; iii) a comparison of the performance of the proposed hybrid model in relation to the LSTM neural network, evaluating the gain in performance with the proposed methodology.

This article is divided as follows: section II presents the methodology used, including the definition of the study area and the proposed forecasting pipeline; section III describes the results obtained with the proposed hybrid model, comparing its performance with that of the LSTM alone; section IV discusses the benefits and limitations of the study; and finally, section V presents the conclusions and directions for future work.

II. METHODOLOGY

The methodology used in this study was divided into four phases. Firstly, in **Data Collection and Preparation**, the region chosen as the geographical context and the methodology for obtaining GPP data are discussed. Then, in **Time Series Decomposition**, the decomposition followed by the pre-processing of the data is explained. Next, in **Forecasting Models**, the structure of the proposed model is commented on, as is the description for hybrid modeling. Finally, in **Performance Evaluation Metrics**, the concepts relating to the evaluation metrics used are explored. Figure 1 visually presents the methodology of this article.

A. DATA COLLECTION AND PREPARATION

This section presents the methods for obtaining the variables needed to calculate the GPP, including its final calculation. Firstly, in **Study Area**, the motivation for choosing the study area is reinforced, along with geographical and environmental details of the region. In **MERRA-2 and MOD15A2H Data**, the main data sets used are discussed, including the methods for acquiring these data. Finally, in **Gross Primary Productivity Calculation**, the algorithm used to calculate the GPP is commented on.

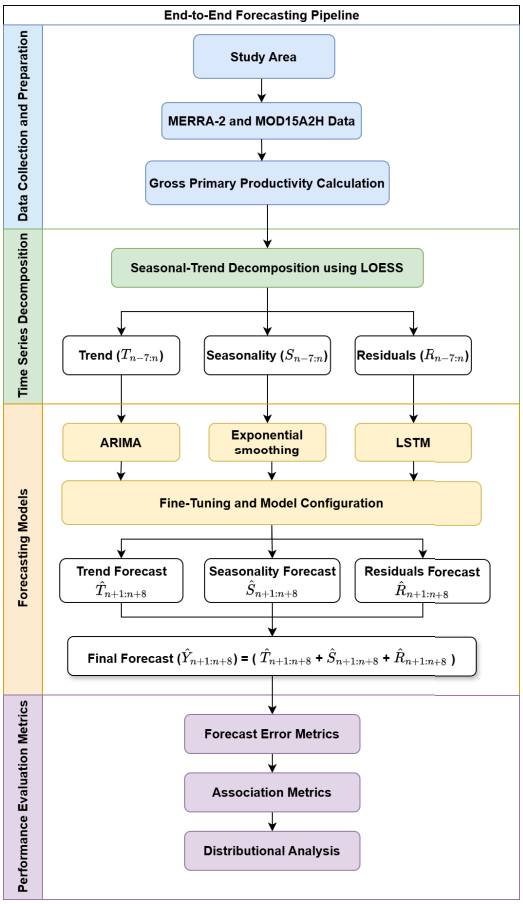

FIGURE 1. End-to-End forecast proposed pipeline flowchart. The division on the Y axis represents the subsections of this article's methodology. The colored blocks within each division represent subsubsections, while the white blocks represent the data obtained.

1) STUDY AREA

Considering the recent literature (2020-2023) of studies aimed at the quantitative and qualitative analysis of carbon concentration in the Amazon rainforest [15], around 42% of the studies are carried out within the Brazilian Amazon. The spatial heterogeneity of the dynamics of the carbon cycle in the Amazon rainforest is already known [44], [45] and the lack of studies in other regions can generate scientific gaps in certain parts of the Amazon.

In this context, the Peruvian Amazon, in particular, is home to vast areas of tropical forests and unique ecosystems, including vast deposits of peat, which play a crucial role in long-term carbon storage [46], accounting for approximately 20% of global carbon [47]. Despite its importance, according to [47], this region remains under-represented in studies, which limits understanding, especially of the carbon and methane cycle, as well as its responses to hydro-meteorological variations. The study therefore highlights the

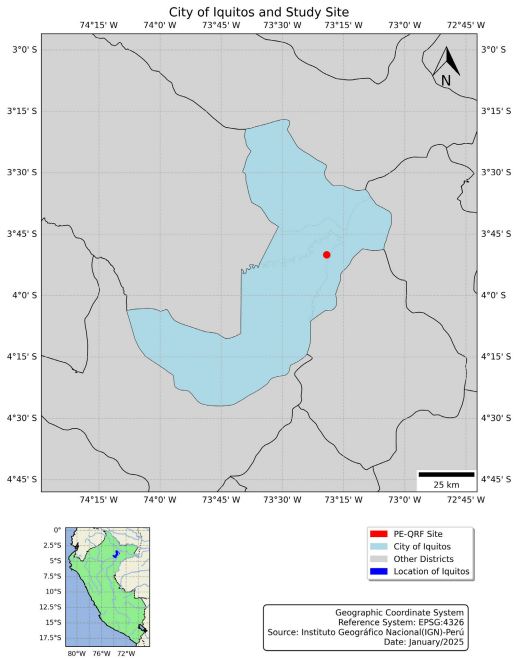

FIGURE 2. Overview of the study area.

need to increase observations and research in the Peruvian Amazon in order to quantify and understand the energy balance characteristics of these systems.

Therefore, in order to contribute to the advancement of knowledge in this region, the PE-QFR site (Figure 2), which is located in the Quistococha Federal Reserve, near the district of Iquitos, in the municipality of Loreto, Peru, (QFR, 3° 50' S, 73° 19' W) emerges as a strategic location for mitigating climate change in the region. According to [47], the region represents an important carbon dioxide sink, with a net absorption of -465 gC m^2 in 2018 and -462 gC m^2 in 2019, which highlights its role in mitigating climate change.

According to the land cover classification provided by the MCD12 product [48], vegetation is mostly classified as evergreen broadleaved forests. The region of the site has minimum temperatures of 22.9 °C and maximum temperatures of 31.8 °C during its rainy season and 22.5 °C and 32.7 °C minimum and maximum temperatures during its dry season, with average rainfall of 810 mm and 545 mm, respectively, during the aforementioned seasons [47].

2) MERRA-2 AND MOD15A2H DATA

The daily GPP dataset used to carry out the experiments in this article was developed based on the MERRA-2 [49] reanalysis dataset, which is widely used to calculate the GPP [50], [51], and the MOD15A2H product. This process followed the methodology exhaustively detailed in the MOD17 user manual [26], which is also used to generate the MOD17A2H [52] products, which are made available to the public at 8-day intervals.

The Google Earth Engine[1] platform was used to acquire the variables, using the dataset entitled *M2T1NXSLV* [53] and *M2T1NXRAD* [54], referring to MERRA-2, and MOD15A2H.061. The data collected from MERRA-2 consisted of the daily minimum temperature (T_{min}) and average temperature (T_{mean}) at a height of 10 meters, incident photosynthetically active radiation (PAR), obtained from 45% of the variable referring to the shortwave flux entering the surface [26], water vapor mixing ratio at a height of 10 meters (q_{v10m}) and atmospheric pressure (P). With the MOD15A2H, only data on the fraction of photosynthetically active radiation (fPAR) was collected.

Next, the Actual Vapor Pressure (AVP) and Saturation Vapor Pressure (SVP) variables were obtained using Equations 1 and 2, respectively. The vapor pressure deficit (VPD) was obtained from Equation 3.

$$\text{AVP} = \frac{q_{v10m} \cdot P}{0.622 + 0.379 \cdot q_{v10m}} \tag{1}$$

$$\text{SVP} = 610.7 \cdot \exp\left(\frac{17.38 \cdot T_{mean}}{239 + T_{mean}}\right) \tag{2}$$

$$\text{VPD} = \text{SVP} - \text{AVP} \tag{3}$$

3) GROSS PRIMARY PRODUCTIVITY CALCULATION

To combine the variables in order to obtain the GPP, we used the software that implements the algorithm used in MOD17A2H, which was developed by [50] and is available in a repository on the Github[2] code versioning platform, in the Python programming language.

The algorithm follows a methodology based on radiation use efficiency (ϵ) (Equation 4), which is calculated by multiplying a maximum efficiency factor (ϵ_{max}), obtained from the biome properties table (BPLUT), with scalars resulting from a linear ramp function applied to the variables T_{min} and VPD. The maximum and minimum limits of this function are provided by BPLUT, resulting in $f(T_{\min})$ and $f(VPD)$. Finally, the GPP is calculated using Equation 5.

$$\epsilon = \epsilon_{max} \times f(T_{\min}) \times f(V) \tag{4}$$

$$GPP = \epsilon \times PAR \times fPAR \tag{5}$$

B. TIME SERIES DECOMPOSITION

Environmental time series often present complex patterns and non-linear dynamics that make them difficult to model using simplified approaches. These factors emerge through human-environment interactions, climate variability and ecological interactions. In the Amazon biome, GPP is a variable widely recognized for its complex seasonal dynamics, characterized by fluctuations associated with environmental factors at multiple temporal and spatial scales, especially in the Amazon region [23].

Decomposition methods, used primarily in exploratory data analysis, are decisive techniques for analyzing time

[1] https://earthengine.google.com/
[2] https://github.com/arthur-e/MOD17

series that exhibit complex patterns, as they separate the structural components into distinct structures, facilitating subsequent analysis of each aspect of the time series [55], [56], [57]. In a forecasting context, [58] points out that decomposing the time series into isolated structures can be beneficial, as it eliminates the presence of noise and any stochastic variability in the parts, making it easier to extrapolate each component.

1) SEASONAL-TREND DECOMPOSITION USING LOESS (STL)

Time series decomposition methods include STL decomposition, which separates a time series into three components: Trend, Seasonality and Residuals. Considered a filter procedure, it uses locally estimated scatterplot smoothing (LOESS), operating in a more robust way to outliers compared to the traditional local polynomial (LP) method, acting through an iterative procedure applying a weighted LP smoothing to the original series [59], [60]. The original series is returned following the representation of Equation 6, where y_t represents the value of the original series y at time t, T represents the trend component, S represents the seasonal component and R represents the residual component of the decomposition.

$$y_t = T_t + S_t + R_t \tag{6}$$

To carry out the decomposition, the STL operates through two recursive, nested loops. Each iteration in the inner loop updates the trend and seasonality components through a sequential procedure. The outer loop operates by computing robustness weights; these weights are used to ensure robustness against anomalies in the trend and seasonality components, by changing the smoothing steps with a robust version of LOESS [37], [60].

After decomposing the time series using the STL method, the GPP data was divided chronologically to apply different modeling approaches. For the ARIMA and ES models, the set was divided into 85% for training and 15%. This division was chosen in order to maximize the amount of information for training the statistical models, which depend on a precise adjustment of their coefficients in order to understand the long-term time series. For the LSTM, due to the need for a validation set, the division used was: 70% for training 15% for validation and 15% for testing. This allocation was selected in order to allow appropriate adjustments to the weights and hyperparameters of the LSTM, as well as monitoring the network's ability to generalize.

C. FORECASTING MODELS

In the systematic review carried out by [61], it is highlighted that capturing the patterns, trend and seasonality of the historical data set is used to make accurate forecasts and comments that decomposing the series can be beneficial as it helps to identify individual patterns present in the data.

In order to deal with the various characteristics of the data, after STL decomposition, this study adopted three models with the aim of improving the forecasting of GPP variability. In this section, the details of each of these models are presented: ARIMA, with its theoretical concept and specific application; ES, discussed in terms of its implementation and necessary adjustments; and LSTM, discussed in terms of its concept and training configuration.

Finally, Model Configuration presents the proposed hybrid model, which integrates the approaches discussed - STL, ARIMA, ES and LSTM. In addition to detailing its configuration, the forecast horizon and the optimization of the LSTM hyperparameters are discussed.

1) AUTOREGRESSIVE INTEGRATED MOVING AVERAGE (ARIMA)

ARIMA is a statistical model used for analyzing and forecasting time series. This model expresses a stationary time series as ARIMA(p,d,q), where p represents the order of the autoregressive coefficient, i.e. the past observations (lags) used in the model, d represents the degree of differentiation required to achieve stationarity and q the order of the moving average coefficient. The modeling represents a linear combination of the past values of the stationary series and random errors, guided by the autocorrelation (ACF) and partial autocorrelation (PACF) functions to model the stochastic nature of the original series and thus estimate future values [62].

The ARIMA model is widely used in various fields, including financial forecasting [63], climate forecasting [64] and environmental forecasting [65], and is highly relevant in short-term forecasting tasks. In this study, the trend component decomposed by the STL method helps to identify linear patterns in the decomposed trend, which facilitates its modeling with ARIMA, a classical statistical model.

2) EXPONENTIAL SMOOTHING (ES)

Exponential smoothing models are a family of methods that produce forecasts based on weighted averages of past observations, with the associated weighting decreasing as the distance of the observation from the current point [56]. These methods are divided into:

- Simple exponential smoothing (SES): Useful for series with no clear trend or seasonality;
- Double exponential smoothing (or Holt's linear method): Can model the trend of a series;
- Triple exponential smoothing (or Holt-Winters seasonal method): Can model both the trend and seasonality of a time series;

The ES family models are widely recognized and used in various forecasting tasks. Previous studies have successfully applied them both to climate time series forecasts [66] and to hybrid applications aimed at forecasting electricity consumption [67]. Triple exponential smoothing was used to model the seasonal component of the GPP, due to its easy implementation and low computational cost [68], as well as its ability to give more importance to recent

observations for forecasting, making it effective for short horizon forecasts [69], [70].

3) LONG-SHORT TERM MEMORY (LSTM)

First proposed by [71], LSTMs are a type of recurrent neural network (RNN) created to correct the problem of gradient disappearance. This type of network has internal memory, represented by memory blocks with a unit that protects it from the problem mentioned above. This type of behavior allows the neural network to capture long-term patterns, making it an ideal choice for predicting future values based on past events.

Recent studies have already addressed the application of LSTM models in climate variable forecasting tasks [72], highlighting their expertise in modeling complex and non-linear time series. In addition, current research [73], [74] has investigated the performance of LSTM models in hybrid approaches, especially in forecasting tasks for extreme weather events and environmental monitoring. Furthermore, the residuals decomposed by STL often contain non-linear patterns and complex temporal dependencies, which the LSTM recurrent neural network model can capture effectively.

In this study, the implementation of the LSTM library *Tsai*[3], called LSTMPlus [75], was used to carry out the forecasts, with the only change being the automatic implementation in the last layer, in order to guarantee that the forecasts are output in the desired format. This implementation was chosen because the environment provided by the library guarantees a wide variety of specific configurations for creating and testing deep learning models for predicting time series.

In addition, to train the network, the data was previously normalized and Huber's loss function [76] was used to ensure robust training against outliers. In addition, two procedures were used to monitor training: reducing the learning rate when the loss function in the validation set stops decreasing (ReduceLROnPlateau) and ending training early if performance does not improve after a predetermined number of epochs (EarlyStopping). These procedures were used to prevent overfitting during training. It is important to note that the LSTM belonging to the hybrid model, used to model the residual component of the decomposition, will be denoted as $\text{LSTM}_{Residual}$ to differentiate it from the benchmark LSTM model, which uses the same settings.

4) FINE-TUNING AND MODEL CONFIGURATION

In order to carry out the forecasts, it was decided to use 8 past values to forecast 8 future values, ensuring consistency with the structure provided by the MOD17 product for data availability. For the ARIMA and ES models, multi-step forecasting was used to adapt to the structure.

To ensure robustness in the evaluation, a specific cross-validation method for time series was used, called Walk Forward Cross Validation (WFCV) with 3 folds. Traditional cross-validation was not used in the analysis due to its behavior of shuffling the data, which violates the general structure of time series, which follow a chronological order, unlike WFCV which preserves this order by training and testing the model incrementally, using past data to predict the future. Recent studies such as [77] and [78] have used this same method with similar motivation for performance evaluation.

To evaluate the uncertainty of the predictions obtained due to random initialization, the approach based on [22] was used, in which each model was trained a total of 10 times, giving a total of 20 GPP predictions. The interquartile range between the predictions was then calculated and the dispersion of the predictions was taken into account, with the median representing the best prediction of that model.

In addition, the Optuna library was used to acquire the best hyperparameters for both the LSTM networks and the ES model. Optuna is a framework specialized in the automatic search for hyperparameters, providing an efficient environment for finding the best configurations for the proposed model [79]. For its implementation, 100 trials were used to find the parameters of the LSTM and ES models, which are part of the hybrid structure, and 150 trials to find the parameters of the network used for benchmarking, LSTM. For the ARIMA model, the *auto_arima* method was used via the *pmdarima* library, implemented in Python with default settings.

D. PERFORMANCE EVALUATION METRICS

Association and error metrics were used to assess the performance of the models. It is therefore necessary to understand the metrics used in order to better understand the results obtained. This subsection presents the metrics and methods used to evaluate the models, detailing the concepts and reasons for choosing them. Firstly, in Error Metrics, the average error metrics used to evaluate the performance of the models are presented. Next, Distributional Analysis explains the metrics used to analyze the distribution of forecast errors. Finally, Association Metrics discusses the association metrics used to quantify the relationship between predicted and observed values.

1) ERROR METRICS

To evaluate the final forecasts in general, the following metrics were used: Mean Absolute Error (MAE), Root Mean Square Error (RMSE) and Mean Absolute Percentage Error (MAPE). The MAE provides a robust view against outliers of the average magnitude of the errors presented in the forecasts, providing estimates on the same scale as the original set [80]. The RMSE, unlike the MAE, highlights the largest errors, since they are squared before the average is calculated, providing a sensitive estimate for analyzing large deviations observed in the predictions [81]. Finally, MAPE offers an intuitive measure of the model's performance in relative terms, demonstrating the magnitude of the discrepancy

[3]https://timeseriesai.github.io/tsai/

between predicted and actual values [82]. Their respective concepts are detailed below:

- MAE: It represents the average of the absolute differences between the actual observations, denoted as y, and the predictions made by forecasting models, denoted by $\hat{y}$. The MAE is obtained from Equation 7.

$$\text{MAE} = \frac{1}{n}\sum_{i=1}^{n}|y_i - \hat{y}_i| \tag{7}$$

- RMSE: It measures the square root of the mean of the squared differences between the actual observations and those predicted by a regression model. The RMSE is obtained from Equation 8.

$$\text{RMSE} = \sqrt{\frac{1}{n}\sum_{i=1}^{n}(y_i - \hat{y}_i)^2} \tag{8}$$

- MAPE: It measures the absolute difference between actual observations and predictions in percentage terms, through the proportion of the magnitude of error observed in relation to the actual value. MAPE is obtained from Equation 9.

$$MAPE = \frac{1}{n}\sum_{i=1}^{n}\left|\frac{y_i - \hat{y}_i}{y_i}\right| \tag{9}$$

2) ASSOCIATION METRICS

Measures of association quantify the relationship between two variables, mainly assessing the strength and direction of this relationship. In this study, the coefficients of determination (R^2) and Pearson's correlation coefficient (r) were used. The R^2 was chosen because it provides an explanatory measure of how much of the variability in the time series is explained by the proposed model, and has already been used in other studies as an evaluation metric in environmental contexts [23], [83], [84]. In a complementary way, r shows the direction and intensity of the linear relationship between variables, and is often used in environmental studies to evaluate the performance of LSTM models and also to analyze the relationship between climate variables [22], [85].

- R^2: Evaluates how well a linear regression model explains the relationship between variables in terms of the proportion of variance, with a maximum value of 1, which means maximum explanation, zero, no explanation [86], but it can also have negative values when the model fails to explain the variation in the data [87]. The R^2 is obtained from Equation 10, where $\hat{y}$ represents the values predicted by the model and y the actual observations, where $\bar{y}$ is the average of the data set in question.

$$R^2 = 1 - \frac{\sum(y_i - \hat{y}_i)^2}{\sum(y_i - \bar{y})^2} \tag{10}$$

- r: It quantifies the strength and informs the direction of the linear relationship between the variables, ranging from -1 to 1, where the first dictates a perfect negative linear correlation and the second a perfect positive linear correlation. In cases where r is close to zero, it is said that the variables do not have such a relationship [88]. The value of r is obtained from Equation 11.

$$r = \frac{\sum(\hat{y}_i - \bar{\hat{y}})(y_i - \bar{y})}{\sqrt{\sum(\hat{y}_i - \bar{\hat{y}})^2 \sum(y_i - \bar{y})^2}} \tag{11}$$

3) DISTRIBUTIONAL ANALYSIS

As a complement to the analysis carried out with the main metrics, the Skewness and Kurtosis metrics were considered, which are related to the distribution of forecast errors, making it possible to evaluate characteristics such as symmetry and dispersion around a normal distribution. This analysis is relevant because it allows systematic patterns in forecast errors to be determined.

Firstly, the Skewness metric was chosen because it allows us to assess whether there are patterns of underestimation or overestimation in the observed errors, which is essential for assessing whether the model is introducing systematic biases into the forecasts. In addition, this metric has been widely used as a complement to analysis based on traditional metrics in studies evaluating prediction errors in artificial intelligence models [89], [90].

It is important to note that high or negative Skewness values indicate, respectively, an overestimation or underestimation bias in the predictions in relation to the observed values. Skewness is obtained from Equation 12, where N is the number of forecast errors, x_i is the value of the ith error, $\overline{x}$ is the mean and σ is the standard deviation of the forecast errors.

$$Skewness = \frac{1}{N}\sum_{i=1}^{N}\frac{(x_i - \overline{x})^3}{\sigma^3} \tag{12}$$

Kurtosis was used to assess the concentration of errors around the mean, helping to identify distributions with heavy tails compared to a symmetrical distribution. High or very negative values indicate the strong presence of outliers in the forecast errors. This metric is complementary to Skewness and is traditionally used together [89], [90]. Kurtosis is obtained from Equation 13.

$$Kurtosis = \frac{1}{N}\sum_{i=1}^{N}\frac{(x_i - \overline{x})^4}{\sigma^4} \tag{13}$$

III. RESULTS

This section presents the results obtained from the inference of the STL-ARIMA-ES-LSTM model, with the traditional LSTM used as a baseline for comparison. Initially, in **Error and Association**, the general error metrics are discussed. Next, in **Monthly Residual**, the dispersion of errors on a monthly scale is presented. Finally, in **Forecast Error Distribution**, the shape of the error distribution is explored.

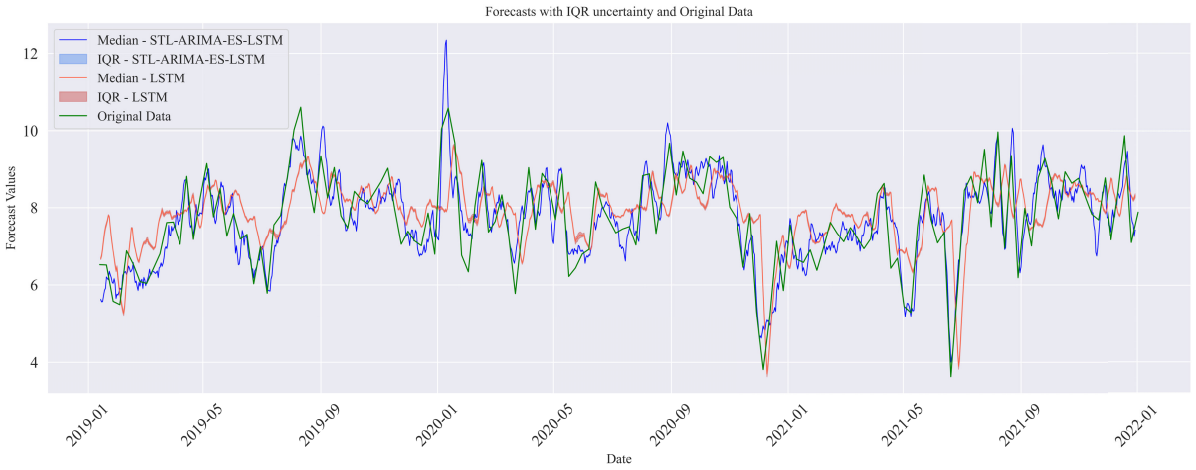

FIGURE 3. Uncertainty associated with the random initialization of the weights of the neural networks. (The image can be enlarged, maintaining its high resolution.)

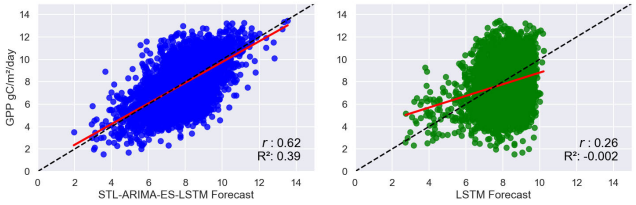

FIGURE 4. Regression analysis between the observed variable and the prediction of each model.

A. ERROR AND ASSOCIATION

Figure 3 shows a graph comparing the forecasts of each model with the original observations in the last fold, in which a moving average filter was used to make the graph easier to see. The spots around the forecasts indicate the uncertainty interval, represented by the IQR of the forecasts around the median over the 10 forecasts made by each model. It can be seen from the image that the proposed model consistently outperformed the LSTM alone, with spots referring to uncertainty less visible throughout the series. With regard to error metrics, the proposed model (STL-ARIMA-ES-LSTM) consistently outperformed the isolated LSTM, with RMSE of 1.69 gC/m^2/day, MAE of 1.35 gC/m^2/day and MAPE of 0.20%, while the isolated LSTM obtained 2.16 gC/m^2/day, 1.78 gC/m^2/day and 0.27%.

With regard to the association metrics, Figure 4 shows the dispersion of the data, with a fitted regression line, between the observed GPP and that predicted by each model. The dotted black line indicates the ideal case, in which the predictions correspond exactly to the values in the observations. The proposed model showed a better quality of fit in relation to the observations, with correlation coefficient $r = 0.62$ and $R^2 = 0.39$. In contrast, the LSTM showed an inferior fit, with r and R^2 equal to 0.26 and -0.002, respectively.

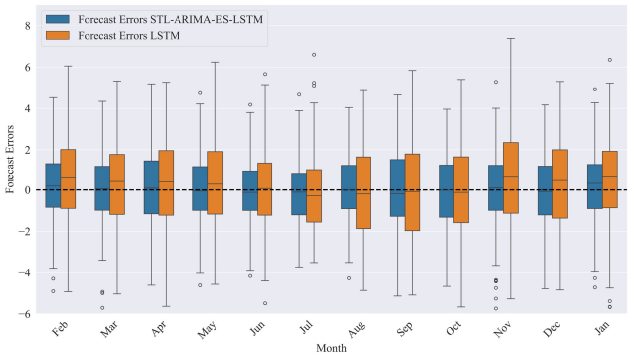

FIGURE 5. Distribution of forecast errors on a monthly scale. The dashed line serves as a reference for the scenario in which predicted values match the observed ones.

B. MONTHLY FORECAST ERROR

Figure 5 shows the dispersion of the forecast errors for each of the models on a monthly scale, looking for possible seasonal patterns in the forecast errors. A reference line at zero was included to indicate the ideal case of the forecasts having the same values as the observations. It can be seen that the forecast errors of the proposed hybrid model (in blue) remain close to the reference line in most of the months analyzed, while the LSTM forecast errors (in orange) show greater dispersion and total amplitude.

In addition, the proposed model showed a monthly median more concentrated at zero, with the greatest deviation from the median in January with a GPP error value of 0.32 gC/m^2/day, it also showed consistently lower extreme values, with the greatest positive extremes observed in the months of November (5.27 gC/m^2/day) and April (5.18 gC/m^2/day), and negative extremes in March (-5.71 gC/m^2/day) and November (-5.74 gC/m^2/day).

With the LSTM, the greatest deviations from the median were observed in January and November, with GPP values of

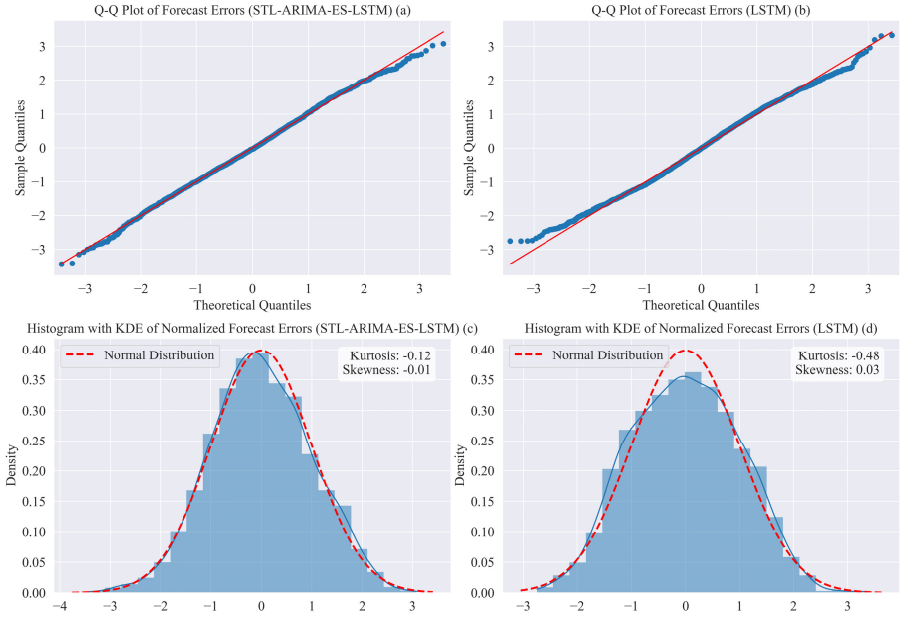

FIGURE 6. Distribution of models. The image can be enlarged while maintaining its high resolution.

0.71 gC/m^2/day and 0.70 gC/m^2/day, and it also showed a significantly greater range of error, with more dispersed extreme values. The greatest positive extremes for LSTM occurred in November (7.38 gC/m^2/day) and July (6.60 gC/m^2/day), while the negative extremes were recorded in October (-5.66 gC/m^2/day) and April (-5.63 gC/m^2/day).

C. FORECAST ERROR DISTRIBUTION

Figure 6 shows comparisons made between the forecast error distributions and the normal distribution. In this context, Figures 6(a) and 6(b) indicate subtle deviations in the tails of both distributions, with the best fit presented by the proposed model (Figure 6(a)), despite the presence of positive outliers being significant. On the other hand, the LSTM (Figure 6(b)) shows a lower quality of fit, visible in the sharp deviations in both the positive and negative tails.

In addition, Figure 6(c) and Figure 6(d) visually show the histogram and kernel density estimate (KDE) of the forecast errors. It can be seen that, for the hybrid model, the estimated curve is closer to a normal distribution, as evidenced by the kurtosis (-0.12) and asymmetry (-0.01) values, which indicate less deviation from symmetry and the concentration of values around the mean. On the other hand, the LSTM model shows a greater deviation, as evidenced by the kurtosis (-0.48) and asymmetry (0.03), which reinforce the lower adherence of the errors to normality.

IV. DISCUSSION

The results of this study show that the STL-ARIMA-ES-LSTM hybrid model outperforms the traditional LSTM in predicting Gross Primary Productivity (GPP) in the Amazon region. The hybrid model showed a lower absolute error (MAE), root mean square error (RMSE) and absolute percentage error (MAPE), as well as a higher correlation coefficient (r) and R^2, indicating a more faithful representation of GPP variability. These findings suggest that the combination of statistical techniques and machine learning may be more effective in capturing the complex dynamics of the carbon cycle in the Amazon.

STL decomposition proved to be an essential step in improving the GPP forecast, allowing for more efficient modeling of trends and seasonality. The use of ARIMA to model the trend and Exponential Smoothing (ES) for seasonality contributed to reducing noise and improving forecast accuracy, while LSTM was responsible for capturing non-linear patterns in the residual component. These results are in line with previous studies indicating that hybrid models can outperform isolated approaches in complex environmental forecasting [91], [92], [93], [94], [95]. However, it is worth noting that the efficiency of STL decomposition can vary depending on the type of data and the temporal dynamics of the variable studied. In this sense, future research could explore alternative decomposition techniques, such as Fourier analysis or Wavelets, to assess whether the segmentation of the time series can be optimized.

When compared to other studies, it can be observed that approaches based exclusively on machine learning may have limitations in predicting environmental time series due to the difficulty of modeling or predicting extreme events, especially when these events are not included in the training period [96]. Furthermore, the combination of hybrid models has been explored in several areas, such as water quality forecasting [91], [92], ozone concentration forecasting [93], and solar energy generation forecasting [95], reinforcing the relevance of integrated approaches.

Despite the good results, some limitations should be considered. The model relies on reanalysis data (MERRA-2), which can introduce uncertainties, especially in regions with low direct observation coverage. In addition, validation was carried out at a single monitoring site (PE-QFR), which may not reflect the spatial variability of GPP throughout the Amazon [23]. Future studies should explore the application of the model in different regions, as well as integrating high-resolution remote sensing data to improve the spatial representation of the forecast.

With regard to modeling the behavior of the GPP, it can be seen from other studies that in the palm swamp region studied, it manages to be a large CO^2 sink in the wet season [47], with reduced intensity in the dry season due to the closure of leaf stomata to preserve internal water by evaporation, reducing photosynthesis, a pattern also observed in terra firme latifolia vegetation further east in the Amazon, in Brazil [17]. This seasonal pattern was well captured by the model even with only two years of data in the region, however, ongoing climate change is causing changes in the pattern of rainy seasons in the Amazon, as well as an increase in average temperature, which may decrease the effectiveness of the model's forecast, considering only the carbon flux time series.

Future analyses could investigate multivariate forecasts combining GPP models and climate forecasts, using updated temperature and humidity data to detect abrupt changes in carbon uptake. Together, the simulation of future GPP series based on the different warming scenarios provided by the Intergovernmental Panel on Climate Change (IPCC) can provide important perspectives on changes in the different component biomes of the Amazon region as a result of surface warming [97].

Furthermore, the implications of the proposed model go beyond predicting GPP. The improved accuracy of the estimates can contribute to a better understanding of the carbon cycle and provide subsidies for forest conservation policies, such as the REDD+ program, and apply social programs focused on changing the land use of the population in the region of greatest impact, such as in the areas of agricultural frontier and cattle ranching [5], [7]. Incorporating socioeconomic variables, such as deforestation and land use indices, could further refine the model's ability to anticipate changes in the carbon balance [22].

Thus, this study reinforces the potential of hybrid approaches for modeling complex environmental systems and highlights the need for additional research to expand and validate the proposed methodology. With further refinements, this approach could become a valuable tool for environmental monitoring and the development of effective climate change mitigation strategies.

V. CONCLUSION

This study demonstrated the effectiveness of the STL-ARIMA-ES-LSTM hybrid model in forecasting GPP in the Amazon region, surpassing the results obtained by the traditional LSTM network in terms of error, association and distribution metrics. The use of STL decomposition as a pre-processing stage, together with the combination of statistical and machine learning methods, proved to be a promising approach for capturing the complex dynamics of environmental time series, highlighting its potential for application to other variables of climatic interest.

The results presented show the potential of hybrid approaches to solve challenges related to modeling complex environmental systems, especially in regions of high biodiversity and climatic relevance, such as the Amazon. Although the model was applied to the GPP, the methodology can be adapted to other variables critical to the carbon cycle, broadening the scope of application in tropical biomes.

Even so, the study faces limitations, such as the dependence on reanalysis data and the low density of flux towers in the Amazon, factors that restrict validation on broader scales. Future work should explore the integration of remote sensing data with greater temporal and spatial resolution, as well as investigating the application of more advanced models to capture even more complex seasonal patterns.

Furthermore, this study makes a substantial contribution to advancing our understanding of the dynamics of the carbon cycle, offering tools that can support public policies aimed at mitigating climate change and conserving the Amazon rainforest. By reinforcing the importance of the Amazon as a global climate regulator, it is hoped that the results presented here will inspire new research and strategies to protect this essential ecosystem. Finally, to ensure the replication of the results, a repository containing the Python code, dataset and images used in this article has been created and is available in a repository on Github.[4]

ACKNOWLEDGMENT

For open access purposes, the authors have assigned the Creative Commons CCBY license to any accepted version of the article.

REFERENCES

[1] N. A. of Sciences, D. on Earth, L. Studies, B. on Atmospheric Sciences, C. on Extreme Weather Events, and C. C. Attribution, *Attribution of Extreme Weather Events in the Context of Climate Change*. Washington, DC, USA: National Academy Press, 2016.

[2] G. O. Ofremu, B. Y. Raimi, S. O. Yusuf, B. A. Dziwornu, S. G. Nnabuife, A. M. Eze, and C. A. Nnajiofor, "Exploring the relationship between climate change, air pollutants and human health: Impacts, adaptation, and mitigation strategies," *Green Energy Resour.*, vol. 2024, May 2024, Art. no. 100074.

[3] R. Burbidge, C. Paling, and R. M. Dunk, "Adapting Latin American and Caribbean airports to a changing climate: Impacts, challenges and solutions," *Climate Risk Manage.*, vol. 47, 2025, Art. no. 100684.

[4] B. A. Karimi, M. A. Haziq, and A. Hayat, "Specific impacts of climate change on the hydrological patterns and land use dynamics in the arghandab river basin, Kandahar, Afghanistan," *Natural Hazards Res.*, Jan. 2025. [Online]. Available: https://www.sciencedirect.com/science/article/pii/S2666592124000994

[5] A. Pawłowski and P. Rydzewski, "Pathways to carbon neutrality: Integrating energy strategies, policy, and public perception in the face of climate change—A global perspective," *Energies*, vol. 17, no. 23, p. 5867, Nov. 2024.

[4]https://github.com/JeanArthurCostaDias/Hybrid-Structure-Forecasting

[6] J. T. Houghton, B. A. Callander, and S. K. Varney, *Climate Change*. Cambridge, U.K.: Cambridge Univ. Press, 1992.

[7] L. Shen, W. Liu, H. Si, H. Li, N. Li, and F. Yan, "What affects farmers' intention and behavior to mitigate the impact of climate change? Evidence from Hebei province, China," *J. Rural Stud.*, vol. 114, Feb. 2025, Art. no. 103525.

[8] B. Sharma, J. Kumar, A. R. Ganguly, and F. M. Hoffman, "Using image processing techniques to identify and quantify spatiotemporal carbon cycle extremes," in *Proc. IEEE Int. Conf. Data Mining Workshops (ICDMW)*, Nov. 2022, pp. 1136–1143.

[9] E. Rödig, M. Cuntz, A. Rammig, R. Fischer, F. Taubert, and A. Huth, "The importance of forest structure for carbon fluxes of the Amazon rainforest," *Environ. Res. Lett.*, vol. 13, no. 5, May 2018, Art. no. 054013.

[10] R. A. Betts, Y. Malhi, and J. T. Roberts, "The future of the amazon: New perspectives from climate, ecosystem and social sciences," *Phil. Trans. Roy. Soc. B, Biol. Sci.*, vol. 363, no. 1498, pp. 1729–1735, May 2008.

[11] L. F. C. Rezende, A. A. de Castro, C. Von Randow, R. Ruscica, B. Sakschewski, P. Papastefanou, N. Viovy, K. Thonicke, A. Sörensson, A. Rammig, and I. F. A. Cavalcanti, "Impacts of land use change and atmospheric CO_2 on gross primary productivity (GPP), evaporation, and climate in Southern Amazon," *J. Geophys. Research, Atmos.*, vol. 127, no. 8, p. 2021, Apr. 2022.

[12] C. A. Boulton, T. M. Lenton, and N. Boers, "Pronounced loss of Amazon rainforest resilience since the early 2000s," *Nature Climate Change*, vol. 12, no. 3, pp. 271–278, Mar. 2022.

[13] C. H. L. Silva Junior, A. C. M. Pessôa, N. S. Carvalho, J. B. C. Reis, L. O. Anderson, and L. E. O. C. Aragão, "The Brazilian Amazon deforestation rate in 2020 is the greatest of the decade," *Nature Ecology Evol.*, vol. 5, no. 2, pp. 144–145, Dec. 2020.

[14] D. M. Lapola et al., "The drivers and impacts of Amazon forest degradation," *Science*, vol. 379, no. 6630, p. 8622, Jan. 2023.

[15] E. C. G. Araujo, C. R. Sanquetta, A. P. Dalla Corte, A. L. Pelissari, G. A. Orso, and T. C. Silva, "Global review and state-of-the-art of biomass and carbon stock in the Amazon," *J. Environ. Manage.*, vol. 331, Apr. 2023, Art. no. 117251.

[16] H. Gu, G. Yin, Y. Yang, A. Verger, A. Descals, I. Filella, Y. Zeng, D. Hao, Q. Xie, X. Li, J. Xiao, and J. Peñuelas, "Satellite-detected contrasting responses of canopy structure and leaf physiology to drought," *IEEE J. Sel. Topics Appl. Earth Observ. Remote Sens.*, vol. 16, pp. 2427–2436, 2023.

[17] G. de Oliveira, N. A. Brunsell, E. C. Moraes, Y. E. Shimabukuro, G. Bertani, T. V. dos Santos, and L. E. O. C. Aragao, "Gross primary productivity in the northern region of para state, Brazilian amazon, from MOD17 data," in *Proc. IEEE Int. Geosci. Remote Sens. Symp. (IGARSS)*, Jul. 2017, pp. 5822–5825.

[18] Z. Sun, X. Wang, H. Yamamoto, H. Tani, G. Zhong, S. Yin, and E. Guo, "Spatial pattern of GPP variations in terrestrial ecosystems and its drivers: Climatic factors, CO_2 concentration and land-cover change, 1982–2015," *Ecological Informat.*, vol. 46, pp. 156–165, Jul. 2018.

[19] Y. Li, Y. Zhang, and J. Lv, "Interannual variations in GPP in forest ecosystems in Southwest China and regional differences in the climatic contributions," *Ecological Informat.*, vol. 69, Jul. 2022, Art. no. 101591.

[20] Y. Tang, X. Xu, Z. Zhou, Y. Qu, and Y. Sun, "Estimating global maximum gross primary productivity of vegetation based on the combination of MODIS greenness and temperature data," *Ecological Informat.*, vol. 63, Jul. 2021, Art. no. 101307.

[21] L. Huang, M. Liu, Y. Jiang, and R. Tang, "A revised MODIS-GPP algorithm by incorporating seasonal fluctuation of maximum light use efficiency for maize and soybean," in *Proc. IEEE Int. Geosci. Remote Sens. Symp.*, Jul. 2022, pp. 2773–2776.

[22] C. Huang, W. He, J. Liu, N. T. Nguyen, H. Yang, Y. Lv, H. Chen, and M. Zhao, "Exploring the potential of long short-term memory networks for predicting net CO_2 exchange across various ecosystems with multi-source data," *J. Geophys. Res., Atmos.*, vol. 129, p. 2023, Nov. 2023, Art. no. e2023JD040418.

[23] G. B. Costa et al., "WUE and CO_2 estimations by eddy covariance and remote sensing in different tropical biomes," *Remote Sens.*, vol. 14, no. 14, p. 3241, Jul. 2022.

[24] V. H. D. M. Paca, G. E. Espinoza-Dávalos, T. M. Hessels, D. M. Moreira, G. F. Comair, and W. G. M. Bastiaanssen, "The spatial variability of actual evapotranspiration across the Amazon river basin based on remote sensing products validated with flux towers," *Ecological Processes*, vol. 8, no. 1, pp. 1–20, Dec. 2019.

[25] Y. Zhou, S. Niu, L. Xu, and X. Gao, "Spatial analysis of growing season peak control over gross primary production in northern ecosystems using Modis-GPP dataset," in *Proc. IEEE Int. Geosci. Remote Sens. Symp. (IGARSS)*, Jul. 2017, pp. 6221–6224.

[26] F. A. Heinsch, M. Reeves, P. Votava, S. Kang, C. Milesi, M. Zhao, J. Glassy, W. M. Jolly, R. Loehman, C. F. Bowker, J. S. Kimball, R. R. Nemani, and S. W. Running, "GPP and NPP (Mod17a2/a3) products nasa Modis land algorithm," in *Proc. MOD17 User's Guide*, 2003, pp. 1–57.

[27] X. Mao, J. Zheng, L. Liu, W. Han, T. Zhong, and R. Wang, "Evaluation of agricultural drought monitoring through the utilization of vegetation optical depth (VOD) and gross primary productivity (GPP)," in *Proc. 11th Int. Conf. Agro-Geoinformatics (Agro-Geoinformatics)*, Jul. 2023, pp. 1–5.

[28] H. Zhang, H. A. Loaiciga, A. Okujeni, J. Liu, M. Tan, and T. Sauter, "Assessing the impact of extreme climate events on European gross primary production," *Agricult. Forest Meteorol.*, vol. 362, Mar. 2025, Art. no. 110374.

[29] B. Lee, N. Kim, E.-S. Kim, K. Jang, M. Kang, J.-H. Lim, J. Cho, and Y. Lee, "An artificial intelligence approach to predict gross primary productivity in the forests of South Korea using satellite remote sensing data," *Forests*, vol. 11, no. 9, p. 1000, Sep. 2020.

[30] Q. Yang, N. Nie, Y. Wang, X. Wu, W. Liu, X. Ren, Z. Wang, M. Wan, and R. Cao, "Spatial–Temporal correlation considering environmental factor fusion for estimating gross primary productivity in Tibetan grasslands," *Appl. Sci.*, vol. 13, no. 10, p. 6290, May 2023.

[31] A. Wang, M. Zhang, E. Chen, C. Zhang, and Y. Han, "Impact of seasonal global Land surface temperature (LST) change on gross primary production (GPP) in the early 21st century," *Sustain. Cities Soc.*, vol. 110, Sep. 2024, Art. no. 105572.

[32] D. Montero, M. D. Mahecha, F. Martinuzzi, C. Aybar, A. Klosterhalfen, A. Knohl, F. Koebsch, J. Anaya, and S. Wieneke, "Recurrent neural networks for modelling gross primary production," in *Proc. IEEE Int. Geosci. Remote Sens. Symp.*, Jul. 2024, pp. 4214–4217.

[33] J. Xu, Z. Wang, X. Li, Z. Li, and Z. Li, "Prediction of daily climate using long short-term memory (LSTM) model," *Int. J. Innov. Sci. Res. Technol. (IJISRT)*, vol. 9, no. 7, pp. 83–90, Jul. 2024.

[34] Z. Xiong, Z. Zhang, H. Gui, P. Zhu, Y. Sun, X. Zhou, K. Xiao, and Q. Xin, "Predicting time series of vegetation leaf area index across North America based on climate variables for land surface modeling using attention-enhanced LSTM," *Int. J. Digit. Earth*, vol. 17, no. 1, Dec. 2024, Art. no. 2372317.

[35] Y. Bo, X. Li, K. Liu, S. Wang, H. Zhang, X. Gao, and X. Zhang, "Three decades of gross primary production (GPP) in China: Variations, trends, attributions, and prediction inferred from multiple datasets and time series modeling," *Remote Sens.*, vol. 14, no. 11, p. 2564, May 2022.

[36] S. Öztürk and A. Emir, "Estimations of green house gases emissions of Turkey by statistical methods," *Konya J. Eng. Sci.*, vol. 12, pp. 138–149, Jan. 2024.

[37] Z. Ouyang, P. Ravier, and M. Jabloun, "STL decomposition of time series can benefit forecasting done by statistical methods but not by machine learning ones," *Eng. Proc.*, vol. 5, no. 1, p. 42, Jul. 2021.

[38] L. Xu, Y. Ou, J. Cai, J. Wang, Y. Fu, and X. Bian, "Offshore wind speed assessment with statistical and attention-based neural network methods based on STL decomposition," *Renew. Energy*, vol. 216, Nov. 2023, Art. no. 119097.

[39] S. Arslan, "A hybrid forecasting model using LSTM and prophet for energy consumption with decomposition of time series data," *PeerJ Comput. Sci.*, vol. 8, p. e1001, Jun. 2022.

[40] S. J. Taylor and B. Letham, "Forecasting at scale," *Amer. Statistician*, vol. 72, no. 1, pp. 37–45, 2018.

[41] J. Nasir, M. Aamir, Z. U. Haq, S. Khan, M. Y. Amin, and M. Naeem, "A new approach for forecasting crude oil prices based on stochastic and deterministic influences of LMD using ARIMA and LSTM models," *IEEE Access*, vol. 11, pp. 14322–14339, 2023.

[42] U. M. Sirisha, M. C. Belavagi, and G. Attigeri, "Profit prediction using ARIMA, SARIMA and LSTM models in time series forecasting: A comparison," *IEEE Access*, vol. 10, pp. 124715–124727, 2022.

[43] Y.-C. Jin, Q. Cao, K.-N. Wang, Y. Zhou, Y.-P. Cao, and X.-Y. Wang, "Prediction of COVID-19 data using improved ARIMA-LSTM hybrid forecast models," *IEEE Access*, vol. 11, pp. 67956–67967, 2023.

[44] L. Xu, S. S. Saatchi, Y. Yang, R. B. Myneni, C. Frankenberg, D. Chowdhury, and J. Bi, "Satellite observation of tropical forest seasonality: Spatial patterns of carbon exchange in Amazonia," *Environ. Res. Lett.*, vol. 10, no. 8, Aug. 2015, Art. no. 084005.

[45] R. Albright, A. Corbett, X. Jiang, E. Creecy, S. Newman, K.-F. Li, M.-C. Liang, and Y. L. Yung, "Seasonal variations of solar-induced fluorescence, precipitation, and carbon dioxide over the Amazon," *Earth Space Sci.*, vol. 9, no. 1, p. 2021, Jan. 2022.

[46] E. N. Honorio Coronado et al., "Intensive field sampling increases the known extent of carbon-rich Amazonian peatland pole forests," *Environ. Res. Lett.*, vol. 16, no. 7, Jul. 2021, Art. no. 074048.

[47] T. J. Griffis, D. T. Roman, J. D. Wood, J. Deventer, L. Fachin, J. Rengifo, D. Del Castillo, E. Lilleskov, R. Kolka, R. A. Chimner, J. Del Aguila-Pasquel, C. Wayson, K. Hergoualc'h, J. M. Baker, H. Cadillo-Quiroz, and D. M. Ricciuto, "Hydrometeorological sensitivities of net ecosystem carbon dioxide and methane exchange of an Amazonian palm swamp peatland," *Agricult. Forest Meteorol.*, vol. 295, Dec. 2020, Art. no. 108167.

[48] M. Friedl and D. Sulla-Menashe, "MCD12Q1-MODIS/Terra+Aqua land cover type yearly L3 global 500m SIN grid," NASA EOSDIS Land Processes Distributed Active Archive Center, Sioux Falls, SD, USA, Tech. Rep., 2022. [Online]. Available: https://doi.org/10.5067/MODIS/MCD12Q1.006

[49] *MERRA-2: 2d, 1-Hourly, Time-Averaged, Single-Level, Assimilation, Single-Level Diagnostics (Don't short) V5.12.4. Greenbelt, MD, USA, Goddard Earth Sciences Data and Information Services Center (GES DISC)*, GMAO, Greenbelt, MD, USA, 2015.

[50] K. A. Endsley, M. Zhao, J. S. Kimball, and S. Devadiga, "Continuity of global MODIS terrestrial primary productivity estimates in the VIIRS era using model-data fusion," *J. Geophys. Res., Biogeosciences*, vol. 128, no. 9, Mar. 2023, Art. no. e2023JG007457.

[51] N. Madani and N. Parazoo, "Global monthly GPP from an improved light use efficiency model, 1982-2016," ORNL DAAC, Oak Ridge, TN, USA, Tech. Rep. 1982-2016, 2020.

[52] R. Myneni, Y. Knyazikhin, and T. Park, "MOD15A2H-MODIS/Terra leaf area Index/FPAR 8-Day L4 global 500m SIN grid," NASA EOSDIS Land Processes Distributed Active Archive Center, Sioux Falls, SD, USA, Tech. Rep., 2015. [Online]. Available: https://doi.org/10.5067/MODIS/MOD15A2H.061

[53] *MERRA-2 M2T1NXSLV: 2D, 1-Hourly, Time-Averaged, Single-Level, Assimilation, Single-Level Diagnostics (Don't short) V5.12.4. Greenbelt, MD, USA, Goddard Earth Sciences Data and Information Services Center (GES DISC)*, GMAO, Greenbelt, MD, USA, 2015.

[54] *MERRA-2 M2T1NXRAD: 2D, 1-Hourly, Time-Averaged, Single-Level, Assimilation, Radiation Diagnostics (Don't short) V5.12.4. Greenbelt, MD, USA, Goddard Earth Sciences Data and Information Services Center (GES DISC)*, GMAO, Greenbelt, MD, USA, 2015.

[55] Q. Wen, Z. Zhang, Y. Li, and L. Sun, "Fast RobustSTL: Efficient and robust seasonal-trend decomposition for time series with complex patterns," in *Proc. 26th ACM SIGKDD Int. Conf. Knowl. Discovery Data Mining*, Aug. 2020, pp. 2203–2213.

[56] R. Hyndman and G. Athanasopoulos, *Forecasting: Principles and Practice*, 2nd ed., Melbourne, Vic, Australia: OTexts, 2018.

[57] M. West, "Time series decomposition," *Biometrika*, vol. 84, no. 2, pp. 489–494, 1997.

[58] M. Theodosiou, "Forecasting monthly and quarterly time series using STL decomposition," *Int. J. Forecasting*, vol. 27, no. 4, pp. 1178–1195, Oct. 2011.

[59] F. Dama and C. Sinoquet, "Time series analysis and modeling to forecast: A survey," 2021, *arXiv:2104.00164*.

[60] R. B. Cleveland, "STL: A seasonal-trend decomposition procedure based on loess," *J. Off. Statist.*, vol. 6, no. 1, pp. 3–73, 1990.

[61] H. Kaur and H. Kaur, "A comprehensive review on time series forecasting techniques," *JETIR*, vol. 10, pp. 103–111, May 2023.

[62] S. L. Ho and M. Xie, "The use of ARIMA models for reliability forecasting and analysis," *Comput. Ind. Eng.*, vol. 35, nos. 1–2, pp. 213–216, Oct. 1998.

[63] P. Mondal, L. Shit, and S. Goswami, "Study of effectiveness of time series modeling (Arima) in forecasting stock prices," *Int. J. Comput. Sci., Eng. Appl.*, vol. 4, no. 2, pp. 13–29, Apr. 2014.

[64] N. Shivhare, A. K. Rahul, S. B. Dwivedi, and P. K. S. Dikshit, "ARIMA based daily weather forecasting tool: A case study for Varanasi," *MAUSAM*, vol. 70, no. 1, pp. 133–140, Nov. 2021.

[65] A. Fernández-Manso, C. Quintano, and O. Fernández-Manso, "Forecast of NDVI in coniferous areas using temporal ARIMA analysis and climatic data at a regional scale," *Int. J. Remote Sens.*, vol. 32, no. 6, pp. 1595–1617, Mar. 2011.

[66] M. Heydari, H. Benisi Ghadim, M. Rashidi, and M. Noori, "Application of holt-winters time series models for predicting climatic parameters (Case study: Robat garah-bil station, Iran)," *Polish J. Environ. Stud.*, vol. 29, no. 1, pp. 617–627, 2020.

[67] C. Liu, B. Sun, C. Zhang, and F. Li, "A hybrid prediction model for residential electricity consumption using holt-winters and extreme learning machine," *Appl. Energy*, vol. 275, Oct. 2020, Art. no. 115383.

[68] Q. T. Tran, L. Hao, and Q. K. Trinh, "A comprehensive research on exponential smoothing methods in modeling and forecasting cellular traffic," *Concurrency Comput., Pract. Exper.*, vol. 32, no. 23, p. 5602, Dec. 2020.

[69] J. W. Taylor, "An evaluation of methods for very short-term load forecasting using minute-by-minute British data," *Int. J. Forecasting*, vol. 24, no. 4, pp. 645–658, Oct. 2008.

[70] W. Christiaanse, "Short-term load forecasting using general exponential smoothing," *IEEE Trans. Power App. Syst.*, vols. PAS–90, no. 2, pp. 900–911, Mar. 1971.

[71] S. Hochreiter, "Long short-term memory," in *Neural Computation*. Cambridge, MA, USA: MIT Press, 1997.

[72] C. Broni-Bedaiko, F. A. Katsriku, T. Unemi, M. Atsumi, J.-D. Abdulai, N. Shinomiya, and E. Owusu, "El Niño-Southern oscillation forecasting using complex networks analysis of LSTM neural networks," *Artif. Life Robot.*, vol. 24, no. 4, pp. 445–451, Dec. 2019.

[73] K. Venkatachalam, P. Trojovský, D. Pamucar, N. Bacanin, and V. Simic, "DWFH: An improved data-driven deep weather forecasting hybrid model using transductive long short term memory (T-LSTM)," *Expert Syst. Appl.*, vol. 213, Mar. 2023, Art. no. 119270.

[74] T. Q. Vo, S.-H. Kim, D. H. Nguyen, and D.-H. Bae, "LSTM-CM: A hybrid approach for natural drought prediction based on deep learning and climate models," *Stochastic Environ. Res. Risk Assessment*, vol. 37, no. 6, pp. 2035–2051, Jun. 2023.

[75] I. Oguiza, "TSAI—A state-of-the-art deep learning library for time series and sequential data," Github, San Francisco, CA, USA, Tech. Rep., 2023. [Online]. Available: https://doi.org/10.1007/978-1-4612-4380-9_35

[76] P. J. Huber, "Robust estimation of a location parameter," in *Breakthroughs in Statistics: Methodology and Distribution*. Cham, Switzerland: Springer, 1992, pp. 492–518.

[77] P. Krishan, R. Mohapatra, and S. Sengupta, "Adversarial attacks and defenses in multivariate time-series forecasting for smart and connected infrastructures," 2024, *arXiv:2408.14875*.

[78] H. Hwang, J.-H. Jang, E. Lee, H.-S. Park, and J. Y. Lee, "Prediction of the number of asthma patients using environmental factors based on deep learning algorithms," *Respiratory Res.*, vol. 24, no. 1, p. 302, Dec. 2023.

[79] T. Akiba, S. Sano, T. Yanase, T. Ohta, and M. Koyama, "Optuna: A next-generation hyperparameter optimization framework," in *Proc. 25th ACM SIGKDD Int. Conf. Knowl. Discovery Data Mining*, Jul. 2019, pp. 2623–2631.

[80] T. Chai and R. R. Draxler, "Root mean square error (RMSE) or mean absolute error (MAE)?" *Geoscientific Model Develop. Discuss.*, vol. 7, no. 1, pp. 1525–1534, 2014.

[81] M. Z. Naser and A. Alavi, "Insights into performance fitness and error metrics for machine learning," 2020, *arXiv:2006.00887*.

[82] U. Khair, H. Fahmi, S. A. Hakim, and R. Rahim, "Forecasting error calculation with mean absolute deviation and mean absolute percentage error," *J. Phys., Conf. Ser.*, vol. 930, Dec. 2017, Art. no. 012002.

[83] Z. Xia, "Analysis of the spatiotemporal variation characteristics and driving factors of land vegetation GPP in a certain region of Asia," *Open J. Ecology*, vol. 14, no. 6, pp. 523–543, 2024.

[84] M. Liu, J. Peñuelas, A. T. Trugman, G. Vargas G, L. Yang, and W. R. L. Anderegg, "Diverging responses of terrestrial ecosystems to water stress after disturbances," *Nature Climate Change*, vol. 15, no. 1, pp. 73–79, Jan. 2025.

[85] Q. Zeng, X. Lu, S. Chen, X. Cui, H. Zhang, and Q. Zhang, "Comparing the performance of vegetation indices for improving urban vegetation GPP estimation via eddy covariance flux data and Landsat 5/7 data," *Ecological Informat.*, vol. 86, May 2025, Art. no. 103023.

[86] D. Chicco, M. J. Warrens, and G. Jurman, "The coefficient of determination R-squared is more informative than SMAPE, MAE, MAPE, MSE and RMSE in regression analysis evaluation," *PeerJ Comput. Sci.*, vol. 7, p. e623, Jul. 2021.
[87] O. M'hamdi, S. Takács, G. Palotás, R. Ilahy, L. Helyes, and Z. Pék, "A comparative analysis of XGBoost and neural network models for predicting some tomato fruit quality traits from environmental and meteorological data," *Plants*, vol. 13, no. 5, p. 746, Mar. 2024.
[88] P. R. B. Guimarães, "Análise de Correlação e medidas de associação," in *Proc. Curitiba, Universidade Federal do Paraná*, 2017, pp. 1–26.
[89] A. Alhendi, A. S. Al-Sumaiti, M. Marzband, R. Kumar, and A. A. Z. Diab, "Short-term load and price forecasting using artificial neural network with enhanced Markov chain for ISO new England," *Energy Rep.*, vol. 9, pp. 4799–4815, Dec. 2023.
[90] E. S. Solano, P. Dehghanian, and C. M. Affonso, "Solar radiation forecasting using machine learning and ensemble feature selection," *Energies*, vol. 15, no. 19, p. 7049, Sep. 2022.
[91] N. Noori, L. Kalin, and S. Isik, "Water quality prediction using SWAT-ANN coupled approach," *J. Hydrol.*, vol. 590, Nov. 2020, Art. no. 125220.
[92] H. Lu and X. Ma, "Hybrid decision tree-based machine learning models for short-term water quality prediction," *Chemosphere*, vol. 249, Jun. 2020, Art. no. 126169.
[93] M. K. AlOmar, M. M. Hameed, and M. A. AlSaadi, "Multi hours ahead prediction of surface ozone gas concentration: Robust artificial intelligence approach," *Atmos. Pollut. Res.*, vol. 11, no. 9, pp. 1572–1587, Sep. 2020.
[94] D. Duncan and C. Räth, "Optimizing the combination of data-driven and model-based elements in hybrid reservoir computing," *Chaos, Interdiscipl. J. Nonlinear Sci.*, vol. 33, no. 10, Oct. 2023, Art. no. 103109.
[95] C. Vennila, A. Titus, T. S. Sudha, U. Sreenivasulu, N. P. R. Reddy, K. Jamal, D. Lakshmaiah, P. Jagadeesh, and A. Belay, "Forecasting solar energy production using machine learning," *Int. J. Photoenergy*, vol. 2022, pp. 1–7, Apr. 2022.
[96] J. M. Frame, F. Kratzert, D. Klotz, M. Gauch, G. Shalev, O. Gilon, L. M. Qualls, H. V. Gupta, and G. S. Nearing, "Deep learning rainfall–runoff predictions of extreme events," *Hydrol. Earth Syst. Sci.*, vol. 26, no. 13, pp. 3377–3392, Jul. 2022.
[97] C. Vera, G. Silvestri, B. Liebmann, and P. González, "Climate change scenarios for seasonal precipitation in South America from IPCC-AR4 models," *Geophys. Res. Lett.*, vol. 33, no. 13, pp. 1–4, Jul. 2006.

JEAN A. C. DIAS is currently pursuing the bachelor's degree in computer engineering with the Federal University of Pará (UFPA), Belém, Brazil. Since 2023, he has been a member of the Operational Research Laboratory (LPO), working as a Scientific Initiation Fellow. He focuses on research at the intersection of data science and environmental analysis, with an emphasis on machine learning applied to remote sensing.

PEDRO H. DO V. GUIMARÃES received the bachelor's degree in computer engineering from the Federal University of Pará (UFPA), Castanhal Campus, in 2025. He is currently pursuing the master's degree with the Electrical Engineering Graduate Program (PPGEE), Belém, PA, in the area of applied computing, with a research line in computational intelligence.

From 2021 to 2024, he was a Scientific Initiation Scholarship Holder, working on the analysis of socioeconomic and environmental indicators in the Amazon with an interdisciplinary perspective, as a member of the Anthropization Laboratory (L'ANTRO) and the Operational Research Laboratory (LPO). His research interests include data science, machine learning, remote sensing, geoinformatics, and ecology.

WILLIANE G. S. PEREIRA is currently pursuing the bachelor's degree in information systems with the Federal University of Pará (UFPA), Belém, Brazil. Since 2023, she has been working in research as a Scientific Initiation Scholarship Holder with the Operational Research Laboratory (LPO), UFPA, contributing to the development of digital solutions for social purposes.

LEONARDO DE O. TAMASAUSKAS is currently pursuing the bachelor's degree in information systems with the Federal University of Pará (UFPA), Belém, Brazil. Since 2023, he has been a Research Fellow with the Operational Research Laboratory (LPO), UFPA, focusing on the application of artificial intelligence in remote sensing. His work involves developing advanced models to improve deforestation detection and estimate carbon fluxes in the Amazon using machine learning techniques and satellite image processing. He actively contributes to scientific publications, advancing research in geoinformatics, and environmental monitoring.

MARIVAN S. GOMES was born in May 1968. He received the degree in engineering from the Federal University of Amazonas, in 1994. He is currently pursuing the Ph.D. degree in electrical engineering with the Federal University of Pará (UFPA). He is a Professor with the State University of Amazonas. He has expertise in electrical engineering, with an emphasis on telecommunications systems, and works primarily in the areas of robotics, computer vision, UAVs, embedded systems, and industrial automation.

ALAN B. S. CORRÊA received the degree in computer engineering from the Federal University of Pará (UFPA), in 2023, where he is currently pursuing the master's degree in electrical engineering with PPGEE, conducting research in telecommunications, focusing on 5G and 6G networks, and applied computing, with an emphasis on computer vision. He is a member of the Operational Research Laboratory (LPO).

KARLA FIGUEIREDO received the degree in electrical engineering from UFRJ, and the master's degree in electrical systems and the Ph.D. degree in computer systems from PUC-Rio.

She is currently a Professor with the Department of Computer Science, working both in the graduate program (master's and Ph.D.) in computational sciences and the telemedicine program with UERJ. She is also a Professor with the Department of Electrical Engineering and a Collaborator in the Graduate Program, in addition to coordinating the Laboratory of Intelligence, Robotics, and Applications, PUC-Rio. She has been working in fields, such as artificial intelligence, machine learning, and data science for nearly 26 years. She has published approximately 90 scientific articles and mentored around 75 students at the bachelor's, master's, Ph.D., and postdoctoral levels.

GILSON COSTA (Member, IEEE) received the bachelor's degree in computer engineering from the Pontifical Catholic University of Rio de Janeiro (PUC-Rio), in 1991, the master's degree in computer engineering from the State University of Rio de Janeiro (UERJ), in 2003, with an emphasis on geomatics, and the Ph.D. degree in electrical engineering from PUC-Rio, in 2009, with part of the research conducted with Leibniz University Hannover, Germany.

From 2010 to 2015, he was a Postdoctoral Researcher with the Department of Electrical Engineering, PUC-Rio, and the Institute of Photogrammetry and Geoinformation, Leibniz University Hannover, from 2019 to 2020. He is currently an Associate Professor with the Department of Computer Science and Information Technology, UERJ, and the Coordinator of the Graduate Program in Computational Sciences and Mathematical Modeling, Institute of Mathematics and Statistics (IME/UERJ). His primary research interests include image analysis and computer vision, focusing on remote sensing and deforestation detection in tropical forests.

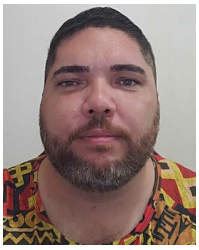

GABRIEL BRITO COSTA received the bachelor's degree in meteorology from the Federal University of Pará, in 2007, the master's degree in meteorology from the Federal University of Alagoas, in 2009, and the Ph.D. degree in sciences (concentration area: applied ecology) from Luiz de Queiroz College of Agriculture (ESALQ) and the Center for Nuclear Energy in Agriculture (CENA), University of São Paulo (USP), in 2015.

He is currently an Associate Professor with the Federal University of Western Pará (UFOPA), specializing in agrometeorology. He is a research and technological development productivity fellow (PQDT), UFOPA. He also serves as a collaborator in several master's programs, including the Postgraduate Program in Anthropogenic Studies of the Amazon (PPGEAA/UFPA), the Postgraduate Program in Biosciences (UFOPA), the Postgraduate Program in Intellectual Property and Technology Transfer for Innovation (PROFNIT/UFOPA), the Postgraduate Program in Natural Resources of the Amazon (PPGRNA/UFOPA), the Postgraduate Program in Climate Sciences (PPGCC/UFRN), and the Postgraduate Program in Biodiversity and Biotechnology (REDE BIONORTE).

FERNANDO A. R. COSTA received the bachelor's degree in tourism from the Federal University of Pará (UFPA), in 2010, the master's degree in development planning from the Graduate Program in Sustainable Development of the Humid Tropics, Núcleo de Altos Estudos Amazônicos (NAEA/UFPA), and the degree in geography from Instituto Federal de Educação, Ciência e Tecnologia do Pará, (IFPA), in 2017.

Currently, he is a School Manager for Elementary Education in Ananindeua, PA, and has published works in the areas of computing, scientific communication, and artificial intelligence. He is a Specialist with the School Management (Universidade Cruzeiro do Sul) and Scientific Communication in the Amazon (NAEA/UFPA). He is involved in the research projects/groups LPO/UFPA, LADES/FACOMP/UFPA-Castanhal, and Territorialização Camponesa na Amazônia, University of the State of Pará (UEPA). His research interests include geography, culture, traditional peoples and communities of the amazon, social cartography, facial expression recognition tools, and violence against women.

MARCOS C. DA R. SERUFFO received the degree in data processing technology from CESUPA, in 2004, a specialization from UFPA, in 2005, the master's degree in computer science and the Ph.D. degree in electrical engineering from UFPA, in 2008 and 2012, respectively, with an emphasis on applied computing.

He completed a Postdoctoral Fellowship with PUC-RJ, in 2020. He is currently an Associate Professor III with UFPA, serving as the Coordinator of the Applied Computing Area of the PPGEE and the Vice-Coordinator of PPGEAA. He has expertise in data science, social technologies, user experience, data mining, computer networks, information technology in education, social network analysis, and natural language processing. Additionally, he coordinates projects funded by CNPq and Capes and is a CNPq Productivity Fellow at Level 2.